Comparison and Analysis of Flux-Switching Permanent-Magnet Double-Rotor Machine With 4QT Used for HEV

Lihong Mo[1,2], Li Quan[1], Xiaoyong Zhu[1], Yunyun Chen[1], Haibing Qiu[1], and K. T. Chau[3]

[1]School of Electrical and Information Engineering, Jiangsu University, Zhenjiang 212013, China
[2]Faculty of Electronic and Electrical Engineering, Huaiyin Institute of Technology, Huai'an 223003, China
[3]Department of Electrical and Electronic Engineering, University of Hong Kong, Hong Kong

The use of double-rotor machines (DRMs) for hybrid electric vehicles (HEVs) has attracted considerable attention due to their compact structure and high torque density. Compared with the conventional four-quadrant transducer (4QT), the proposed flux switching permanent magnet double-rotor machine (FSPM-DRM) has PMs located in the stator, and can offer better performances in terms of magnetic coupling and torque ripple, which are especially important for DRM control in HEVs. This paper presents a comparative analysis of the 4QT and FSPM-DRM by employing the finite element method (FEM). For a fair comparison, two topologies are designed under the same peripheral dimensions, current density, and copper loss. Considering the effect of skewed slots in the 4QT, the corresponding performances are calculated with multi-slice 2-D time-stepping FEM. The simulated results illustrate that the proposed FSPM-DRM offers larger output torque, lower torque ripple, and smaller magnetic coupling than the 4QT. Nevertheless, the eddy current losses in PMs and windings of the FSPM-DRM are higher than those of the 4QT. Experimental results of the FSPM-DRM prototype are also given to verify the validity.

Index Terms—**Double-rotor machine (DRM), finite element method (FEM), flux switching permanent magnet (FSPM) machine, four-quadrant transducer (4QT), hybrid electric vehicle (HEV).**

I. Introduction

With growing concerns on environmental protection and energy conservation, hybrid electric vehicles (HEVs) have gained increasing attention. Currently, the most popular hybrid propulsion system used in HEVs is generally composed of a planetary gear, generator, and motor [1]. This configuration has some advantages such as the relatively high transmission efficiency and mature technology. However, the planetary gear inevitably involves transmission loss, acoustic noise, and regular lubrication. Recently, the electric variable transmission system has been proposed, where various types of double-rotor machines (DRMs) are involved to realize the function of power splitting and coupling without using gearing mechanism. The key of DRMs is the integration of two electric machines, hence to achieve high torque density.

Concerning the DRM structure, the four-quadrant energy transducer (4QT) has been the subject of research for many years since it was first proposed in 2002 [2]. Conventionally, the permanent magnets (PMs) adopted by the 4QT are located in the rotors of two concentric electric machines, resulting in high torque density. Recently, some PM brushless machines with PMs on the stator, such as the flux switching PM machine (FSPM) machine, have been developed [3]. By incorporating the concept of DRM structure into the FSPM, the resulting FSPM-DRM can inherit the merits of simple and robust rotor structure, sinusoidal back electromotive force (EMF) and high power density from the FSPM machine. Nevertheless, compared with the 4QT, the slot opening of the FSPM-DRM is larger and the PMs are closer to windings, which may cause higher loss. Moreover, the PM location may have influence on the magnetic coupling, which is essential to DRM control. Hence, in order to make a full comparison of these two topologies and provide a useful reference for the performance improvement of HEVs, this paper presents a comparative analysis of the 4QT and FSPM-DRM, with emphasis on their magnetic coupling, output torque, loss, and efficiency.

In this paper, first, the 4QT and FSPM-DRM topologies are presented. Then, using the finite element method (FEM), the corresponding electromagnetic performances of these two topologies are analyzed. The temperature impacts on the performances of two topologies are also investigated. Finally, a FSPM-DRM prototype is designed and manufactured to validate the design.

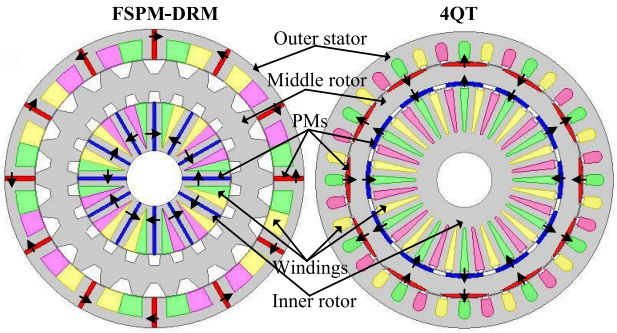

Fig. 1. FSPM-DRM and 4QT topologies.

II. Machine Topologies

Fig. 1 shows the topologies of the proposed FSPM-DRM and conventional 4QT. The outer stator and middle rotor can operate as one machine, which is so-called the outer machine, and the inner rotor and middle rotor can operate as another

Manuscript received March 7, 2014; revised April 17, 2014, April 29, 2014, May 26, 2014, and June 9, 2014; accepted June 10, 2014. Date of current version November 18, 2014. Corresponding author: X. Zhu (e-mail: zxyff@ujs.edu.cn).

Color versions of one or more of the figures in this paper are available online at http://ieeexplore.ieee.org.

Digital Object Identifier 10.1109/TMAG.2014.2331313

TABLE I
MACHINE SPECIFICATIONS

Parameters	FSPM-DRM inner/outer machine	4QT inner/outer machine
Rated current	7.8A (inner) / 5.6A(outer)	
Rated speed	750 rpm / 750rpm	
Outer stator outside diameter	102.4×2 mm	
Outer stator inside diameter	81.9×2mm	
Outer rotor outside diameter	81.3×2mm	
Outer rotor inside diameter	52.6×2mm	65.4×2mm
Inner rotor outside diameter	52×2mm	64.8×2mm
Inner rotor inside diameter	19×2mm	
Airgap length	0.6mm	
Axial length	50 mm	
Phases	3	
Turns per coil	45/50	30/34
Series coils per phase	4	6
Coil area	194 / 125 mm^2	130 / 84 mm^2
Current density	5.1 (inner) / 5.3(outer) A/mm^2	
Stator poles	12/12	36/36
Rotor poles	22/22	12/12
Magnetizing direction	Tangential	Radial
Magnet remanence	1.2 T(inner) / 0.55 T(outer)	
PM volume	40182 mm^3 (inner) / 34320 mm^3(outer)	

machine, namely the inner machine. Each machine can work as a generator or motor. The 4QT is integrated radially by two three-phase 36-slot 12-pole PM synchronous machines. To achieve favorable sinusoidal back EMF waveforms, the outer stator and inner rotor of this 4QT adopt skewed slots [2]. On the other hand, the FSPM-DRM adopts the three-phase 12/22/12-pole structure and is optimized to minimize the torque ripple. The corresponding dimensions are designed to achieve 1 kW for both the inner and outer machines, hence realizing the desired 50% degree of hybridization (DOH, the ratio of electrical power to total power of HEVs). So, for a fair comparison, the 4QT is designed with the same volume of PM material and the same phase current, current density, copper loss, and peripheral dimensions as listed in Table I.

III. ELECTROMAGNETIC PERFORMANCE ANALYSIS

Using the FEM, the electromagnetic performances of the two topologies are analyzed. With the effect of skewed slots in the 4QT, the corresponding electromagnetic performances are calculated using the multi-slice 2-D time-stepping FEM. The skewed angles of the inner rotor and outer stator are 12° and 18°, respectively, and 10 slices are adopted.

A. No-Load Back EMF

By rotating the middle rotor at the rated speed of 750 r/min, the no-load back EMFs of the two topologies are simulated as shown in Fig. 2. It can be observed that the magnitudes of back EMFs in the inner and outer machines of the FSPM-DRM are nearly the same and much greater than those of the 4QT, which is mainly due to the flux-focusing arrangement of the tangentially magnetized PMs in the FSPM-DRM. Furthermore, the back EMFs of FSPM-DRM show better sinusoidal feature than those of 4QT even after adopting skewed slots.

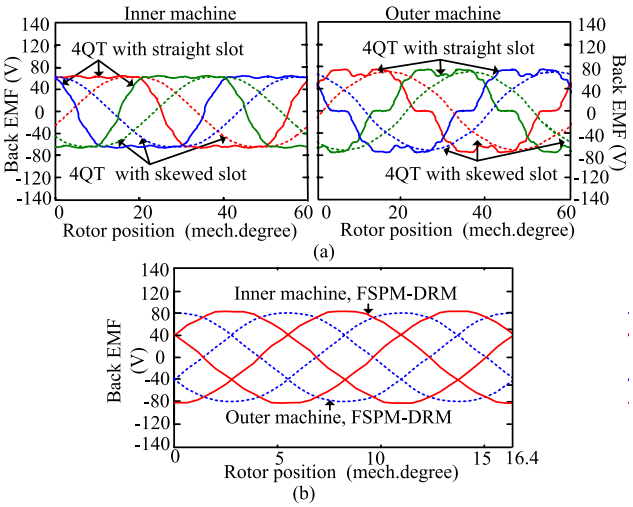

Fig. 2. Back EMF waveforms of two machines at 750 r/min. (a) Back EMFs in 4QT. (b) Back EMFs in FSPM-DRM.

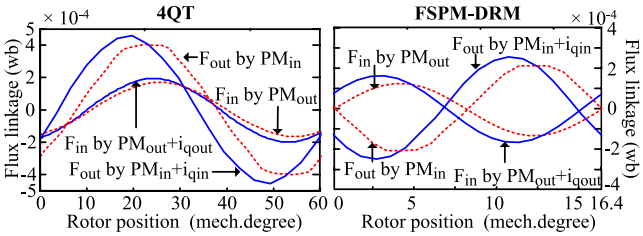

Fig. 3. Coupled flux linkages (I_{qin} = 11 A, I_{qout} = 8 A).

B. Magnetic Coupling Analysis

To investigate the magnetic coupling between the inner and outer machines, the remanence of inner (or outer) PM material is set to zero, and the coupled flux linkages F_{in} in the inner windings (or F_{out} in the outer windings) are simulated when the outer machine (or inner machine) is under the no-load and rated load operations. As shown in Fig. 3, it can be found that the coupled flux linkages of both machines under the no-load and rated load operations are very small, which verifies that the magnetic coupling of two machines can be neglected. Thus, the inner and outer machines of the two topologies can be controlled independently, which is a very important feature for HEV application.

C. Torque

The electromagnetic torque and torque ripple at 750 r/min are calculated as listed in Table II when the copper loss is fixed to 48.4 W for the inner machine and 50.9 W for the outer machine. The FSPM-DRM can produce larger output torque than the 4QT, which is mainly due to the differences between their air gap flux densities, stator and rotor poles, and pole-arc coefficients. The torque ripple ratio K_T (defined as the ratio of the peak-to-peak value to the average value) in Table II indicates that the torque ripples of the 4QT are still higher than those of the FSPM-DRM even after adopting the skewed slots.

TABLE II
AVERAGE TORQUE AND TORQUE RIPPLE
($I_{DIN} = I_{DOUT} = 0$, $I_{QIN} = 11$ A, AND $I_{QOUT} = 8$ A)

Parameters	FSPM-DRM inner/outer machine	4QT inner/outer machine
Average torque	15.5 / 15 N.m	13.4 / 8.9 N.m
K_T	6% / 6%	15.2% / 12.2%

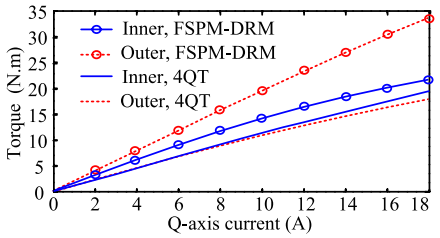

Fig. 4. Torque-current characteristics of 4QT and FSPM-DRM at 750 r/min.

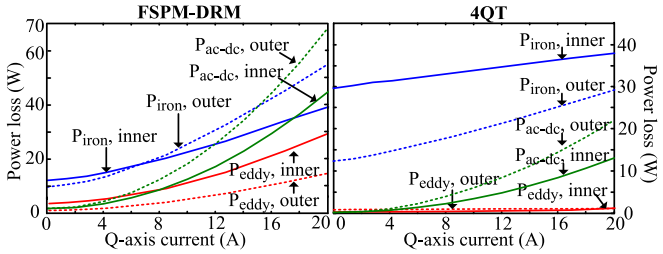

Fig. 5. Power losses in 4QT and FSPM-DRM at 750 r/min.

In addition, the torque-current characteristics of the two topologies are compared in Fig. 4. The outer machine of the FSPM-DRM exhibits the largest output torque capability under the same current. Other three curves show similar torque/current characteristics.

D. Loss and Efficiency

Although the FSPM-DRM offers higher electromagnetic torque than the 4QT, its slot opening is larger and the PMs located in the outer stator and inner rotor may suffer from higher eddy current loss. Thus, the losses and efficiencies of the two topologies are analyzed using the FEM, with particular emphasis on the PM eddy current loss, iron loss, and eddy current loss in windings. The winding eddy current loss is mainly caused by skin and proximity effects, and can be deduced by subtracting the dc copper loss from the predicted total ac copper loss, viz., (ac–dc) loss [4].

In Fig. 5, the inner machine of the 4QT exhibits significantly higher iron loss P_{iron} than other three machines at no-load and is not sensitive to the current. While the outer machine of FSPM-DRM has the largest P_{iron} when the electric loading is large due to the highest inductance and, consequently, more significant armature reaction. The 4QT has negligible PM eddy current loss P_{eddy} since the PMs are located in the outer rotor. At no-load, the outer machine of FSPM-DRM also exhibits low P_{eddy}, whereas the inner machine suffers from high P_{eddy} to its larger air gap flux density. On the other hand, on load, the P_{eddy} of the FSPM-DRM increases significantly with the increase of current, especially for the inner machine. The (ac–dc) copper losses P_{ac-dc} of the FSPM-DRM are higher than those of the 4QT, which is mainly due to the higher flux density and higher frequency produced by the larger rotor pole numbers in the FSPM-DRM. For both topologies, the P_{ac-dc} in the outer machine is higher than that in the inner machine for larger number of turns per phase. The adopted conductors in the inner and outer machines of the two topologies are $\Phi 1.4$ mm $\times$ $L50$ mm and $\Phi 1.18$ mm $\times$ $L50$ mm, respectively.

TABLE III
EFFICIENCIES AT RATED CURRENT UNDER DIFFERENT SPEEDS

Efficiency (%)		FSPM-DRM Inner/outer machine	4QT Inner/outer machine
Speed (rpm)	500	88.1/90.2	91/92.8
	750	91.9/91.5	91.7/90
	1500	91.5/91.3	91.4/87.7
	2000	90.7/90.2	91.2/85

TABLE IV
MATERIAL DATA OF THERMAL MODEL

Material	Thermal Conductivity (W/(m. ^{o}C))	Density (kg/m^3)
Winding	3	8900
Core	40	7900
PM	20	7900

The efficiencies (ignoring the influence of end-effect and mechanical loss) of the two topologies at different speeds can be calculated as listed in Table III. It shows that the FSPM-DRM and 4QT have similar high efficiency except for the outer machine of the 4QT, which can offer high efficiency only within a low speed range.

E. Temperature Impact on Performances

In order to investigate the influence of temperature on the machine performances, the 2-D FE thermal models are built. To simplify the analysis, the assumptions of no axial heat flux and no heat flowing from the inner rotor core to the shaft are made, and the influence of temperature on material is also ignored [2].

The FEM-simulated power losses serve as the heat source for temperature calculation. The transfer of heat by conduction and convection are considered, whereas the radiation phenomena are neglected. Table IV shows the main material properties of the models [5]. The ambient temperature is set to 22 °C. Fig. 6 depicts the PM temperature distributions of the two topologies, in which the FSPM-DRM has slightly higher PM temperature than the 4QT for various operation modes.

Table V summarizes the changes of the losses, output torques, and efficiencies at the rated load when considering the PM temperature rise. It can be found that the rated output torques, losses, and efficiencies all slightly decrease with the temperature rise. After considering the PM temperature rise, the output torques and efficiencies of the FSPM-DRM are still higher than those of the 4QT.

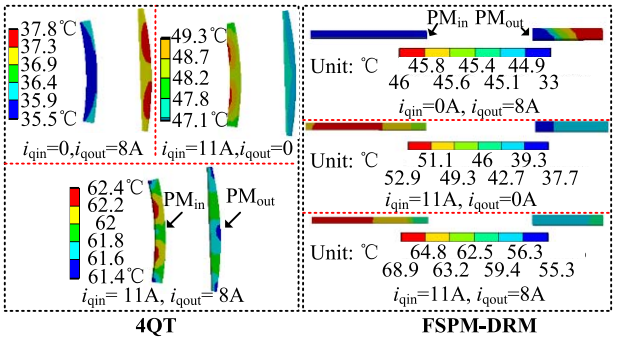

Fig. 6. Temperature distributions in PMs of 4QT and FSPM-DRM at 750 r/min.

TABLE V
PERFORMANCES BEFORE AND AFTER CONSIDERING TEMPERATURE RISE
($I_{DIN} = I_{DOUT} = 0$, $I_{QIN} = 11$ A, AND $I_{QOUT} = 8$ A)

Parameters	FSPM-DRM (Inner/outer)		4QT (Inner/outer)	
	Before	**After**	**Before**	**After**
P_{eddy}(W)	12.9/4.4	12. 6/4	1/0.45	0.98/0.43
P_{iron} (W)	24.2/23.7	24/23.1	34.5/17.7	34.1/17.3
P_{dc}(W)	48.4/50.9	48.4/50.9	48.4/50.9	48.4/50.9
$P_{ac\text{-}dc}$ (W)	13.1/10.6	13/10.4	4/3.8	3.9/3.7
T_{out}(N.m)	14.3/12.3	14.1/12	12.5/7.9	12.4/7.7
P_{out}(W)	1123/966	1107/942	982/620	974/605
η (%)	91.9/91.5	91.9/91.4	91.8/90	91.8/89

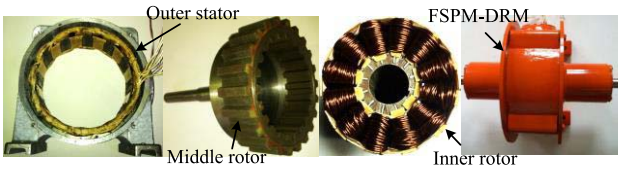

Fig. 7. Machine prototype.

IV. EXPERIMENTAL VALIDATION

In order to validate the design of the proposed FSPM-DRM, a 2 kW prototype has been manufactured. Fig. 7 shows the pictures of this experimental FSPM-DRM. Fig. 8(a) shows the measured no-load back EMFs of the inner and outer machines at the speed of 750 r/min. Compared with the FEM-simulated waveforms shown in Fig. 2(c), there is a good agreement, hence verifying the validity of the machine design. The measured results under various operation modes are shown in Fig. 8(b). It can be observed that the FSPM-DRM can offer high torque during the hybrid driving mode, where the power is provided by both the outer and inner machines. In addition, during the hill climbing condition, the output torque and speed of the inner machine remain the same, and the required output torque is provided by increasing the current of the outer machine. These experimental results agree with the theoretical analysis on the operation principle of HEVs.

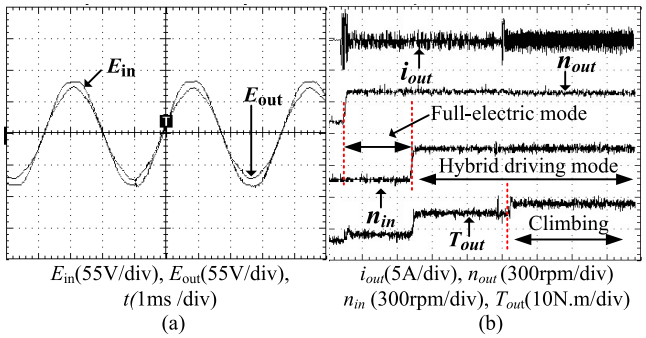

Fig. 8. Measured waveforms and responses at various operation modes. (a) Back EMFs at 750 r/min. (b) Full-electric mode and hybrid driving mode.

Hence, it can be concluded that the FSPM-DRM can be designed to meet all HEV demands.

V. CONCLUSION

This paper has proposed a new FSPM-DRM topology for HEVs, and quantitatively compared the performances of the FSPM-DRM with those of the 4QT. The simulation results have shown that the FSPM-DRM has more sinusoidal back EMF, hence more suitable for brushless ac control. In addition, it offers the advantages of higher torque density and smaller torque ripple, as well as smaller volume and lighter weight. The experimental results have verified that the proposed FSPM-DRM can realize the desired performances and meet the requirements of HEVs for various operation modes. Moreover, this paper has provided some directions for further efficiency optimization of the FSPM-DRM and 4QT, which has a reference value for other DRM designs.

ACKNOWLEDGMENT

This work was supported by the National Natural Science Foundation of China under Grant 51377073 and Grant 51177065.

REFERENCES

[1] K. T. Chau, C. C. Chan, and C. Liu, "Overview of permanent-magnet brushless drives for electric and hybrid electric vehicles," *IEEE Trans. Ind. Electron.*, vol. 55, no. 6, pp. 2246–2257, Jun. 2008.

[2] P. Zheng, R. Liu, P. Thelin, E. Nordlund, and C. Sadarangani, "Research on the cooling system of a 4QT prototype machine used for HEV," *IEEE Trans. Energy Convers.*, vol. 23, no. 1, pp. 61–67, Mar. 2008.

[3] W. Hua, M. Cheng, Z. Q. Zhu, and D. Howe, "Analysis and optimization of back EMF waveform of a flux-switching permanent magnet motor," *IEEE Trans. Magn.*, vol. 23, no. 3, pp. 727–733, Sep. 2008.

[4] L. J. Wu, Z. Q. Zhu, D. Staton, M. Popescu, and D. Hawkins, "Analytical model of eddy current loss in windings of permanent-magnet machines accounting for load," *IEEE Trans. Magn.*, vol. 48, no. 7, pp. 2138–2151, Jul. 2012.

[5] Y. Zhang, J. Ruan, T. Huang, X. Yang, H. Zhu, and G. Yang, "Calculation of temperature rise in air-cooled induction motors through 3-D coupled electromagnetic fluid-dynamical and thermal finite-element analysis," *IEEE Trans. Magn.*, vol. 48, no. 2, pp. 1047–1050, Feb. 2012.